Supporting Information for

Unleashing the Ultra-fast Sodium Ion Storage Mechanisms in Interface-engineered Monolayer MoS_2/C Interoverlapped Superstructure with Robust Charge Transfer Networks

Lili Wang[b], Haitao Zhang*[a], Yanlei Wang[a], Cheng Qian[a], Qiang Dong[b], Chonghai Deng[b], Danfeng Jiang[a], Mengyao Shu[b], Shanshan Pan[a], Suojiang Zhang*[a]

[a] *Beijing Key Laboratory of Ionic Liquids Clean Process, CAS Key Laboratory of Green Process and Engineering, Institute of Process Engineering, Chinese Academy of Sciences, Beijing 100190, P. R. China.*

[b] *School of Energy, Materials and Chemical Engineering, Hefei University, Hefei, Anhui 230601, P. R. China*

***** Corresponding author. Tel.: +86-10-62558174; Fax: +8610-82544875.

E-mail address: htzhang@ipe.ac.cn; sjzhang@ipe.ac.cn

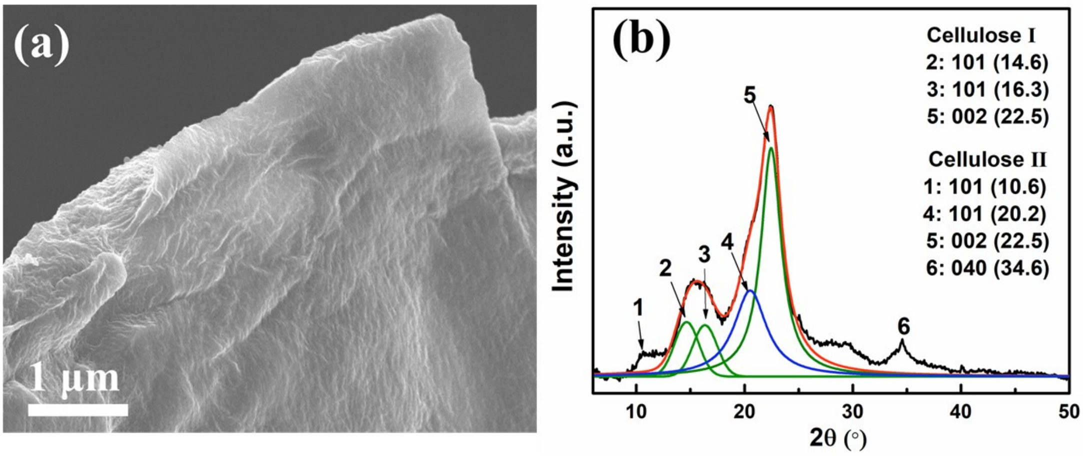

Fig. S1. (a) SEM image and (b) XRD patterns of colloidal bagasse cellulose sheets.

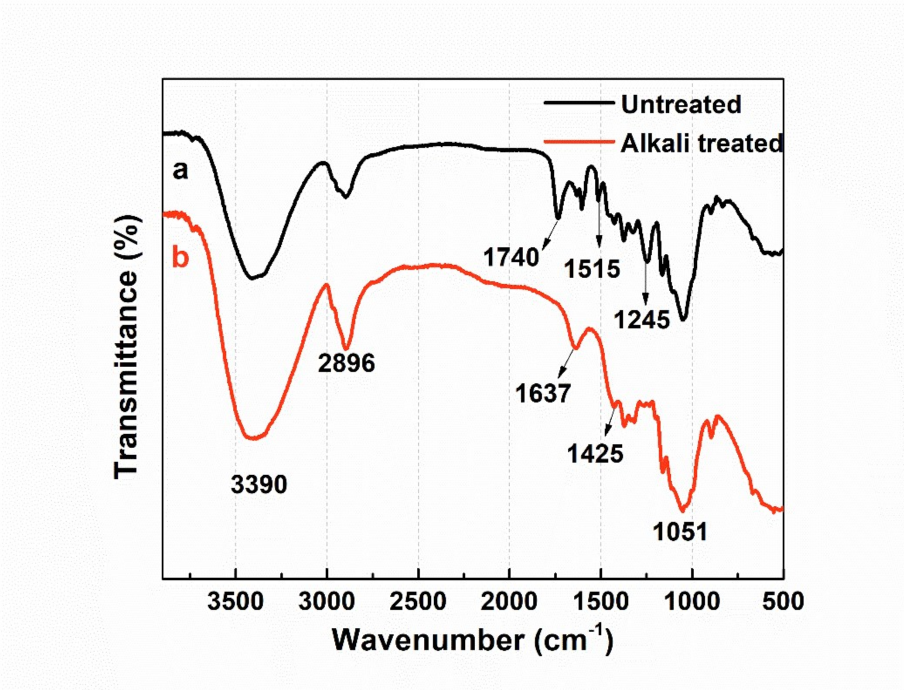

Fig. S2. FTIR spectra of colloidal bagasse cellulose sheets.

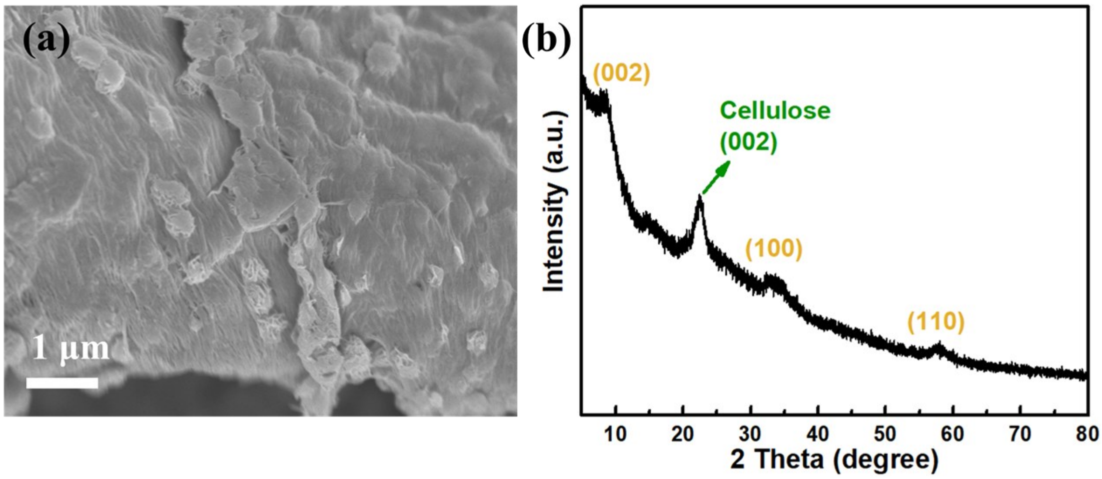

Fig. S3. (a) SEM image and (b) XRD patterns of MoS_2/carbohydrate nanoflowers embedded in the colloidal bagasse sheets (MoS_2/carbohydrate-CBS).

As shown in Fig. S3b, the diffraction peaks at 22.6° is ascribed to (002) planes of cellulose. The diffraction peaks at 32.6° and 57.7° can be indexed to (100) and (110) planes of 2H-MoS_2 (JCPDS card No. 06-0097), respectively. The new peaks at 8.6° (d =1.02 nm) is ascribed to (002) plane. Compared to pristine 2H-MoS_2, the expanded interlayer is probably caused by the insertion of carbohydrate molecules into the adjacent MoS_2 monolayers.

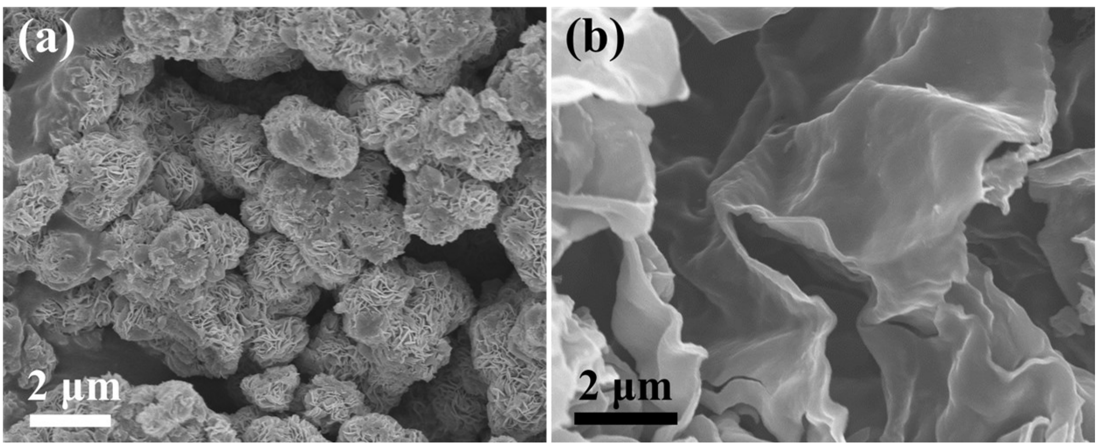

Fig. S4. SEM images of (a) the pristine MoS_2 and (b) the pristine carbon.

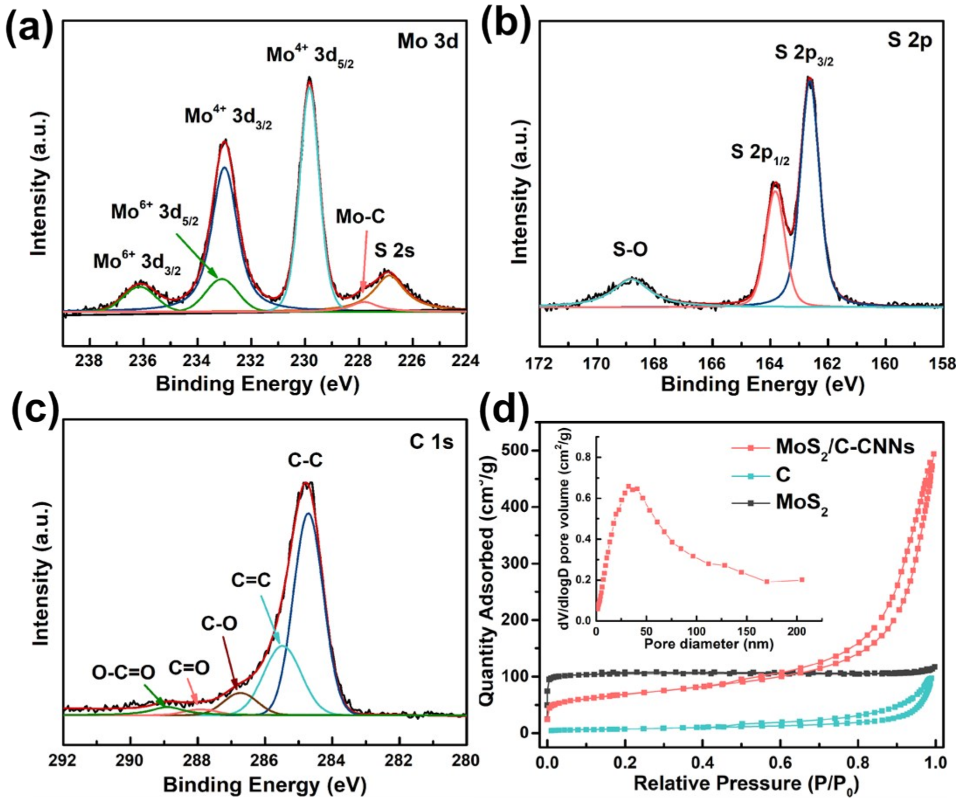

Fig. S5. (a-c) High-resolution XPS spectra of Mo 3d, S 2p and C 1s core level of MoS_2/C-CNNs; (d) N_2 adsorption-desorption isotherms of the MoS_2/C-CNNs, bulk MoS_2 and pure C samples, and inset is the corresponding pore size distribution of MoS_2/C-CNNs.

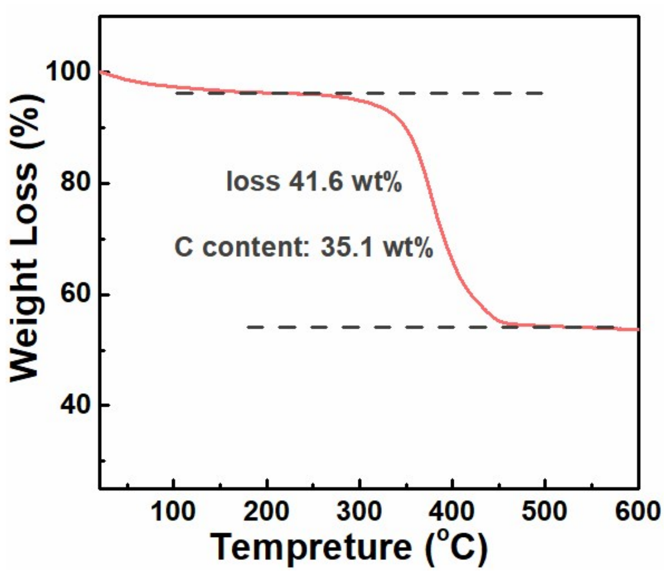

Fig. S6. TGA measurement of MoS_2/C-CNNs.

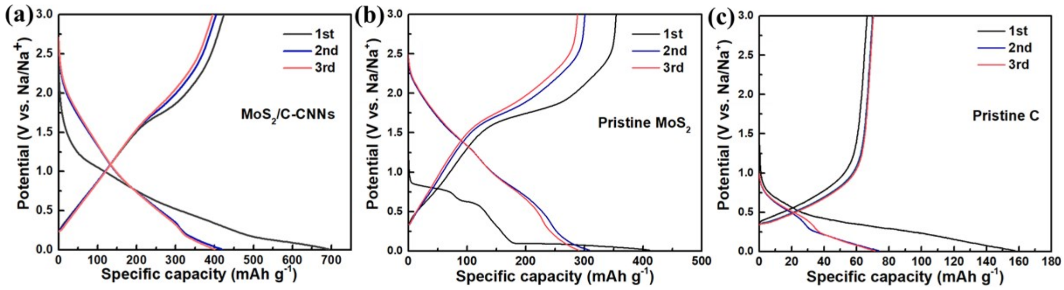

Fig. S7. The first three charge/discharge voltage profiles of (a) the MoS_2/C-CNNs, (b) the pristine MoS_2 and (c) the pristine C electrode at 200 mA g^{-1} between 0.01 and 3.0 V.

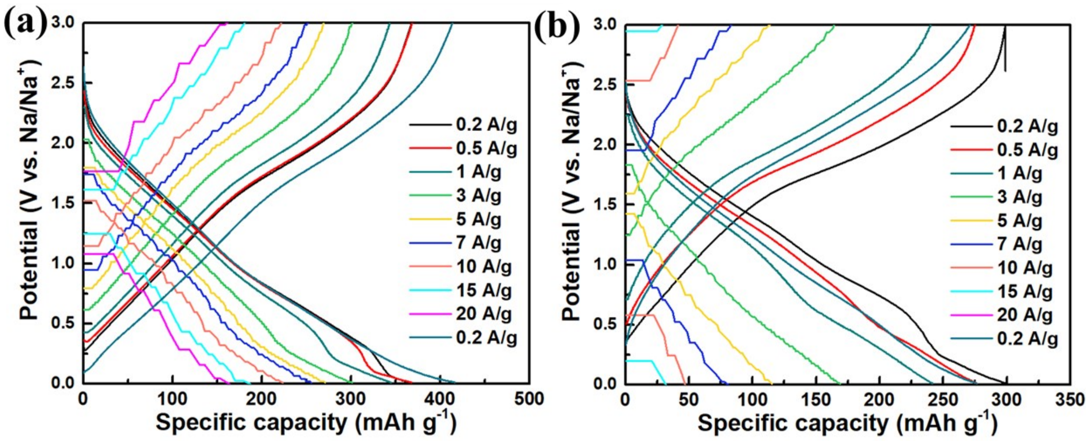

Fig. S8. The charge/discharge voltage profiles of (a) the MoS_2/C-CNNs electrode and (b) the pristine MoS_2 electrode at different current densities.

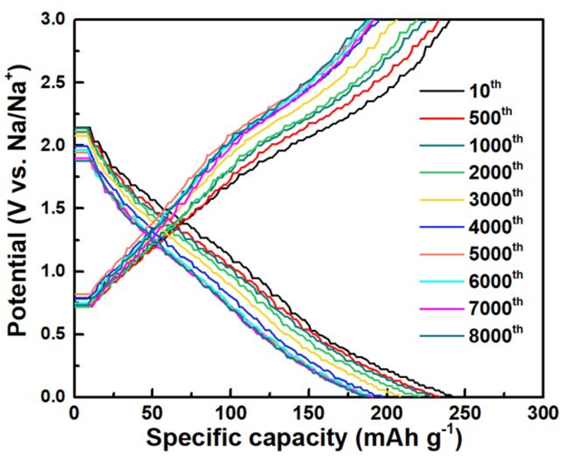

Fig. S9. The charge/discharge voltage profiles of the MoS_2/C-CNNs electrode at different cycles under 5 A g^{-1}.

Table S1. Electrochemical performances of previously reported MoS_2-based SIB anodes in comparison with our MoS_2/C-CNNs

Materials	Cycling data	Rate capability	reference
MoS_2 nanosheets	267/125th@1A/g	226@5A/g	ACS Nano, 13 (2019), 5533-5540.
MoS_2 nanosheets	324/200th@1A/g	253@2A/g	Nano Energy 61 (2019) 361-369.
MoS_2/C hollow nanospheres	262/600th@2A/g	211@10A/g	Nano Energy 51 (2018) 546-555.
MoS_2@carbon nanospheres	150.2/300th@5A/g	204@5A/g	Nano Energy 62 (2019) 299-309.
MoS_2@carbon nanowall	265/1000th@1A/g	235@2A/g	Adv. Funct. Mater. 27 (2017) 1702116.
MoS_2/carbon framework	360/100th@0.1A/g	171@5A/g	Nano Energy 48 (2018) 526-535.
MoS_2/N-Graphene	245/1300th@1A/g	153@20A/g	Adv. Energy Mater. 2018, 8, 1703300
PCNF@MoS_2@PEDOT	410/1000th@2A/g	313@20A/g	Energy Storage Mater. 2020, 25, 114
MoS_2/carbon framework	183.5/3000th@2A/g	~195@15A/g	J. Mater. Chem. A, 2018, 6, 14742
MoS_2/C-CNNs	**193.5/8000th@5A/g**	**223@10A/g 159@20A/g**	**Our work**

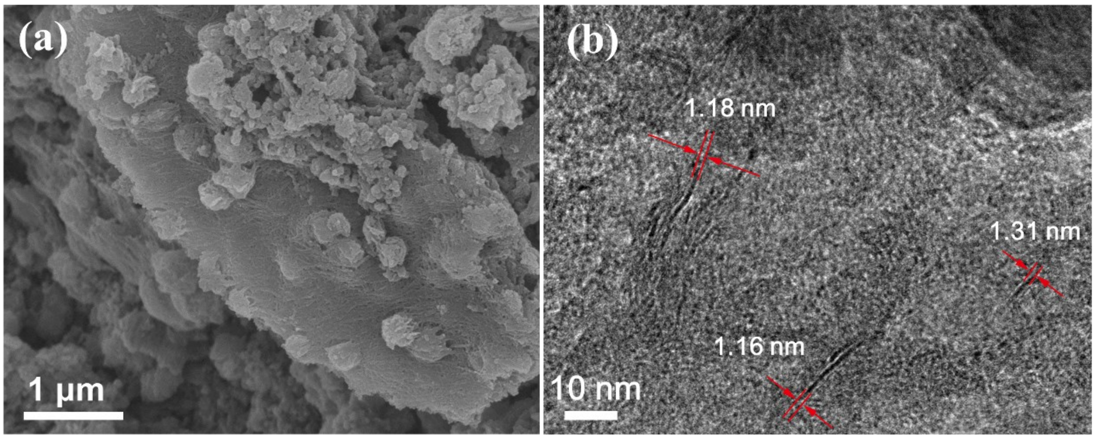

Fig. S10. (a) SEM image of MoS_2/C-CNNs electrode after 1000 cycles; (b) HRTEM image of MoS_2/C-CNNs electrode after 5 cycles.

Table S2. EIS fitting results of pristine MoS_2 and MoS_2/C-CNNs.

	R_s/Ω	R_f/Ω	R_{ct}/Ω	Z_w-R/Ω
Pristine MoS_2 after 10^{th}	6.01	6.13	256.8	454
MoS_2/C-CNNs after 10^{th}	5.39	15.42	50.70	88.3
MoS_2/C-CNNs after 1000^{th}	6.71	12.01	50.46	90.0
MoS_2/C-CNNs after 2000^{th}	6.91	15.29	43.23	129.3
MoS_2/C-CNNs after 4000^{th}	6.52	22.71	37.92	133.4
MoS_2/C-CNNs after 6000^{th}	5.97	26.77	35.24	111.7

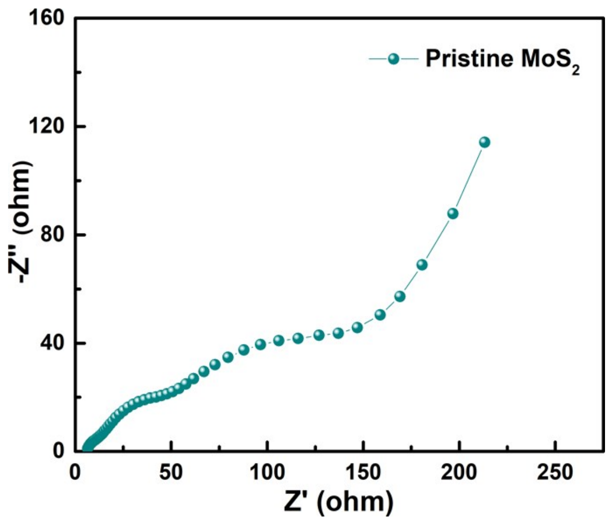

Fig. S11. Nyquist plots of pristine MoS_2 electrode after the 10th circles.

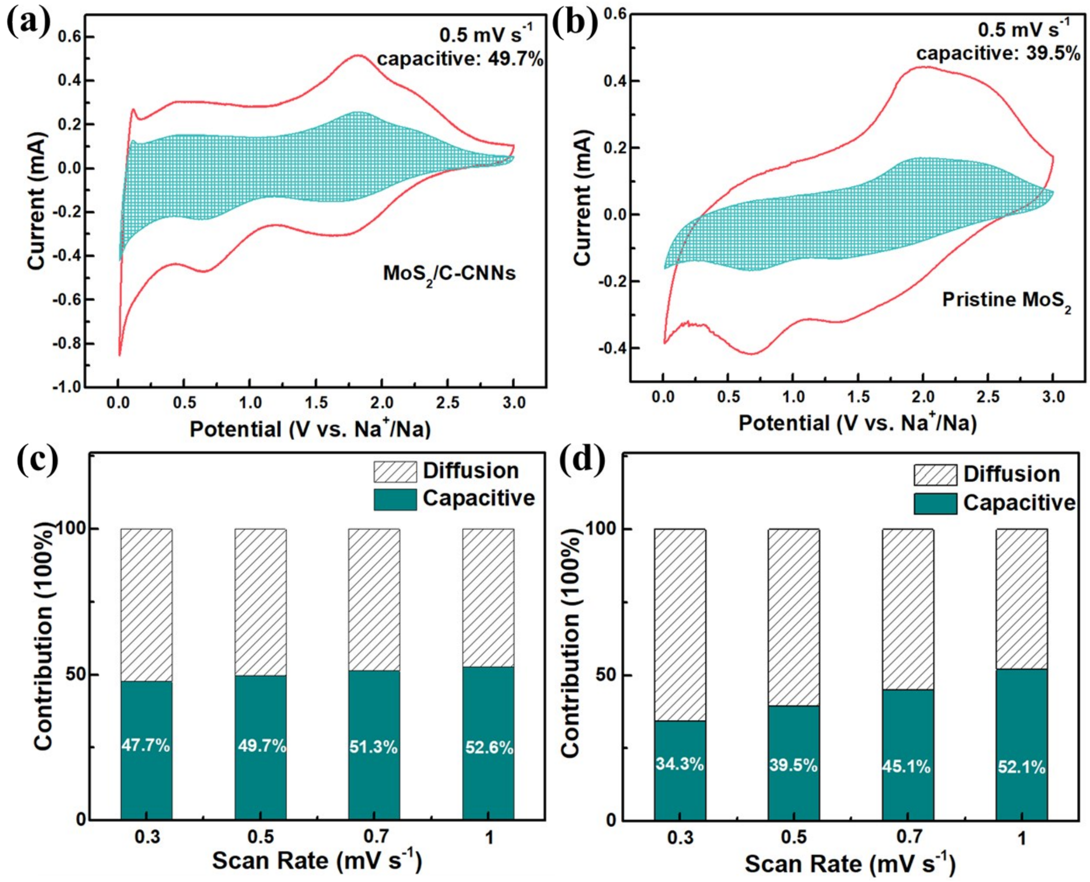

Fig. S12. Separation of the capacitive and diffusion currents in the MoS_2/C-CNNs (a) and the MoS_2 (b) at a scan rate of 0.5 mV s^{-1}, respectively; contribution ratio of the capacitive charge versus scan rate of the MoS_2/C-CNNs (c) and the MoS_2 (d).

The capacitive effect and the diffusion-controlled Na^+ intercalation effects to the sodium storage can be expressed by the equation (Energy Storage Mater., 2018, 14, 129-135): $i(V) = k_1 v + k_2 v^{1/2}$.

$i(V)$ corresponds to the current value at the voltages, v refers to the scan rate, $k_1 v$ refers to the contribution of the capacitive effect provided by the surface-adsorbing charge and $k_2 v^{1/2}$ refers to the solid diffusion control with intercalated/de-intercalated charges.

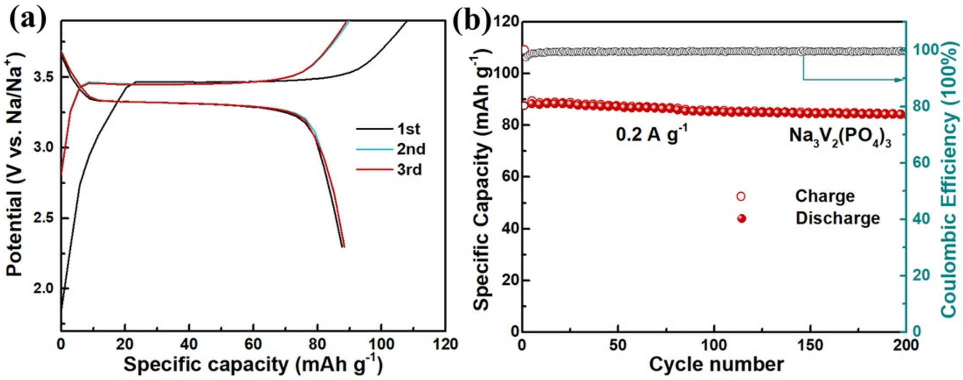

Fig. S13. (a) The first three charge/discharge voltage profiles of the $Na_3V_2(PO_4)_3$ at 0.2 A g^{-1} between 2.3 and 3.9 V; (b) Cycling performance/Coulombic efficiency of the $Na_3V_2(PO_4)_3$ at 0.2 A g^{-1}.

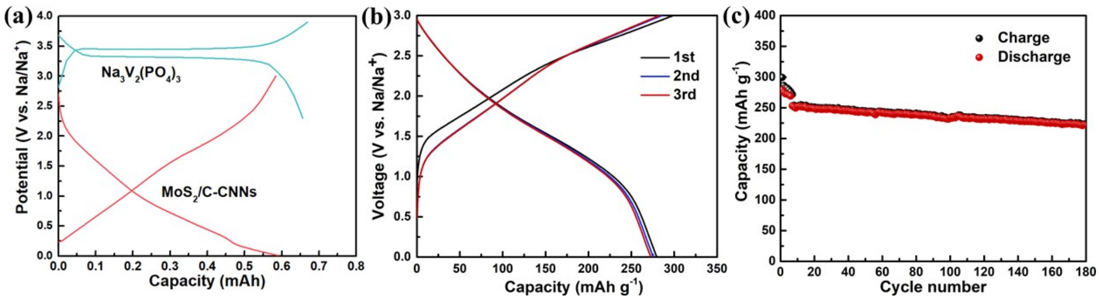

Fig. S14. (a) Charge-discharge profiles of MoS_2/C-CNNs and $Na_3V_2(PO_4)_3$ half cells at a current density of 0.2 A g^{-1}; (b) The charge and discharge profiles of a full-cell at 0.2 A g^{-1} according to the mass of anode materials; (c) Cycling performance of one full-cell at 1 A g^{-1} after first 7 cycles of low current density (0.2 A g^{-1}).